

Impact of Interlayer and Ferroelectric Materials on Charge Trapping during Endurance Fatigue of FeFET with TiN/Hf_xZr_{1-x}O₂/interlayer/Si (MFIS) Gate Structure

Fengbin Tian, Shujing Zhao, Hao Xu, Jinjuan Xiang, Tingting Li, Wenjuan Xiong, Jiahui Duan, Junshuai Chai, Kai Han, Xiaolei Wang, Wenwu Wang, and Tianchun Ye

Abstract—We study the impact of different interlayers and ferroelectric materials on charge trapping during the endurance fatigue of Si FeFET with TiN/Hf_xZr_{1-x}O₂/interlayer/Si (MFIS) gate stack. We have fabricated FeFET devices with different interlayers (SiO₂ or SiON) and Hf_xZr_{1-x}O₂ materials (x=0.75, 0.6, 0.5), and directly extracted the charge trapping during endurance fatigue. We find that: 1) The introduction of the N element in the interlayer suppresses charge trapping and defect generation, and improves the endurance characteristics. 2) As the spontaneous polarization (P_s) of the Hf_xZr_{1-x}O₂ decreases from 25.9 $\mu\text{C}/\text{cm}^2$ (Hf_{0.5}Zr_{0.5}O₂) to 20.3 $\mu\text{C}/\text{cm}^2$ (Hf_{0.6}Zr_{0.4}O₂), the charge trapping behavior decreases, resulting in the slow degradation rate of memory window (MW) during program/erase cycling; in addition, when the P_s further decreases to 8.1 $\mu\text{C}/\text{cm}^2$ (Hf_{0.75}Zr_{0.25}O₂), the initial MW nearly disappears (only ~ 0.02 V). Thus, the reduction of P_s could improve endurance characteristics. On the contract, it can also reduce the MW. Our work helps design the MFIS gate stack to improve endurance characteristics.

Index Terms—Si FeFET, ferroelectric, doped HfO₂, endurance fatigue, charge trapping, interlayer, Hf:Zr ratio.

I. INTRODUCTION

Hafnium-based FeFET is perused due to its excellent characteristics, such as > 10-year retention, low power consumption, fast reading and writing, complete compatibility with the CMOS process, and scaling ability [1-5]. However, the endurance characteristics are generally $10^4\sim 10^5$ [6-13], which is far from the application requirements of memory and

Manuscript received July 6, 2021. This work was supported by the National Natural Science Foundation of China under Grant No. 61904199 and 61904193, and in part by the Open Research Project Fund of State Key Laboratory of ASIC and System under Grant No. KVH1233021. (Corresponding author: Hao Xu, Jinjuan Xiang)

Fengbin Tian, Shujing Zhao, Hao Xu, Jinjuan Xiang, Tingting Li, Wenjuan Xiong, Jiahui Duan, Junshuai Chai, Kai Han, Xiaolei Wang, Wenwu Wang, and Tianchun Ye are with Key Laboratory of Microelectronics Devices and Integrated Technology, Institute of microelectronics, Chinese academy of sciences, Beijing 100029, China. The authors are also with University of Chinese Academy of Sciences, Beijing 100049, China (xuhao@ime.ac.cn; xiangjinjuan@ime.ac.cn).

Kai Han is with Weifang University, Shandong 261061, China.

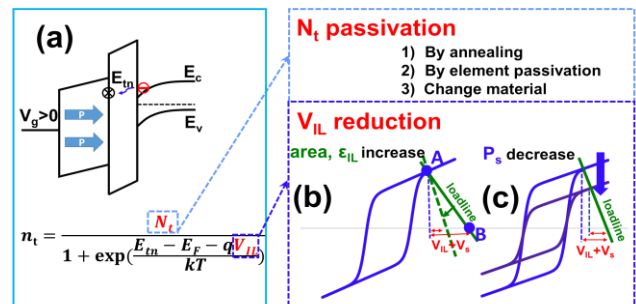


Fig. 1. (a) Energy band diagram of MFIS gate stack showing the charge trapping behavior. The n_t means trapped charge density. (b) and (c) Ferroelectric hysteresis loop and loadline showing the principle of decreasing voltage drop across the interlayer.

computing in-memory application ($>10^{14}$) [14]. Therefore, the study of endurance characteristics has attracted widespread attention.

Significant charge trapping/de-trapping is widely accepted as the origin of endurance fatigue. Thus, effective suppression of charge trapping is rather important to improve endurance characteristics [15-19]. Fig. 1 shows the charge trapping mechanism of the MFIS (TiN/Hf_xZr_{1-x}O₂/interlayer/Si) gate stack. Two parameters determine the charge trapping behavior, i.e., trap density (N_t) and tunneling barrier. Thus, the current method of improving endurance can be summarized as the following two kinds.

The first method is to reduce the N_t . The self-heating effect [7] and high-pressure hydrogen annealing [8] can reduce the N_t . In addition, the introduction of the N element in the SiO₂ interlayer can also effectively suppress trap generation [9, 20, 21]. However, these works claim the trap passivation by measuring the endurance characteristics, but not *directly* measuring the charge trapping behavior.

The second method is to reduce voltage drop on the interlayer (V_{IL}), including i) increasing dielectric constant of interlayer [9, 10, 22, 23], ii) decreasing the area ratio of the ferroelectric and interlayer capacitors [24], iii) eliminating interlayer [5, 25], iv) using Ω -Gate or recessed channel [26, 27], and v) reducing the spontaneous polarization (P_s) of ferroelectric [28-30]. Fig. 1(b) shows the ferroelectric

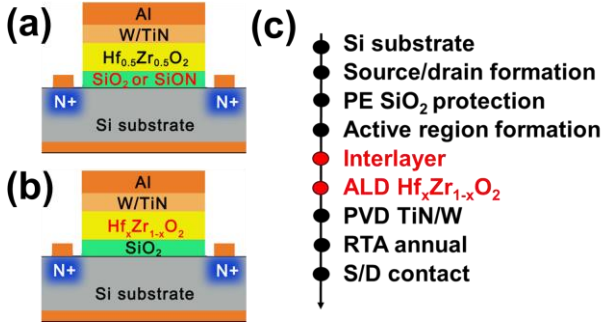


Fig. 2. The schematic of FeFET gate structure of (a) different interlayers and (b) different $\text{Hf}_x\text{Zr}_{1-x}\text{O}_2$ materials, and (c) the fabrication process flow.

hysteresis loop and loadline of the MFIS gate stack to explain the methods (i) and (ii). The intersection between the loadline and hysteresis loop is denoted as ‘A’. The intersection between the loadline and abscissa is denoted as ‘B’. Then the sum of voltage drop on the interlayer (V_{IL}) and surface potential (V_s) is given as the horizontal distance between ‘A’ and ‘B’. Thus, the loadline will become steeper for the methods (i) and (ii). Then the distance decreases, which means that the V_{IL} decreases at the same voltage drop across ferroelectric. Fig. 1(c) shows the ferroelectric hysteresis loop and loadline of the MFIS gate stack for the method (v). By reducing the P_s , the V_{IL} and consequent interlayer electric field (E_{IL}) decrease at the same applied gate voltage. For the method of (v), theoretical predictions have been given [29], while there is no experimental study yet.

In this work, we experimentally study the impact of different interlayers and ferroelectric materials on charge trapping during the endurance fatigue of Si FeFET with $\text{Hf}_x\text{Zr}_{1-x}\text{O}_2$ /interlayer gate stack. For the different interlayer materials, we employ SiO_2 or SiON . For the impact of P_s on endurance fatigue, we employ $\text{Hf}_x\text{Zr}_{1-x}\text{O}_2$ layers by changing the Hf:Zr ratio. We also *directly* measure the charge trapping behavior.

II. EXPERIMENTAL

A. Device fabrication and measurements

The devices were fabricated by using a gate-last process. The silicon substrate used P-type silicon with a resistivity of about 10-12 $\Omega\cdot\text{cm}$. The source/drain was implanted using 40 keV energy with $4 \times 10^{15} \text{ cm}^{-2}$ dose of As ions. The gate structure was W/TiN/ $\text{Hf}_x\text{Zr}_{1-x}\text{O}_2$ /interlayer/Si. The fabricated FeFET devices are summarized as shown in Fig. 2. Fig. 2(a) schematically shows FeFET with different interlayer materials. There are two kinds of interlayers. One is the SiO_2 interlayer, grown by ozone oxidation, and its thickness is about 0.7 nm. The other interlayer is SiON , grown by nitrogen plasma treatment of SiO_2 , and its thickness is about 1.0 nm. Then same $\text{Hf}_{0.5}\text{Zr}_{0.5}\text{O}_2$ ferroelectric was used for different interlayers. The 9 nm $\text{Hf}_{0.5}\text{Zr}_{0.5}\text{O}_2$ was grown by ALD at 300 $^\circ\text{C}$ using tetrakis-(ethylmethylamino)-hafnium (TEMA-Hf) as Hf precursor, tetrakis-(ethylmethylamino)-zirconium (TEMA-Zr) as Zr precursor, and H_2O as O source. Fig. 2(b) schematically shows FeFET with different ferroelectric materials. There are three kinds of $\text{Hf}_x\text{Zr}_{1-x}\text{O}_2$ with $x=0.75$, 0.6, and 0.5. The interlayers are all 0.7 nm SiO_2 . The $\text{Hf}_x\text{Zr}_{1-x}\text{O}_2$ is 9 nm thick. The different Hf:Zr ratios were realized by changing the Hf and

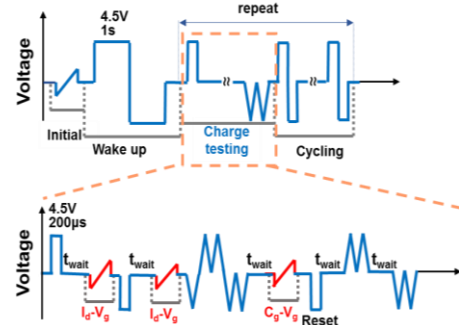


Fig. 3. The details of electrical measurement.

Zr precursor cycles. For all samples, the 10 nm TiN and 75 nm W were deposited by sputtering as the metal gate. Then the ferroelectric phase crystallization was achieved by 550 $^\circ\text{C}$ for 60 s in N_2 to form the orthorhombic phase. Then, the source/drain contacts were defined by lithography, and TiN/Al was used as contact metal. Finally, forming gas annealing at 450 $^\circ\text{C}$ in 5%- H_2 /95%- N_2 was performed. In addition, the capacitor of TiN/ $\text{Hf}_x\text{Zr}_{1-x}\text{O}_2$ /TiN was also fabricated with the same condition as above.

Fig. 3 shows the details of the electrical measurement we used in this work. We used Agilent B1500A and Radiant Precision LC ferroelectric tester to measure the transfer curve I_d-V_g , gate capacitance vs. gate voltage (C_g-V_g), the hysteresis loop, and PUND (Positive Up Negative Down). For MFM capacitors, a triangle wave of 3 V amplitude at 1 kHz was used for hysteresis loop measurement, and a square wave of 3 V amplitude at 1 kHz was used for the endurance characteristics test. For FeFET, AC small-signal measurement at 100 kHz was used for the C_g-V_g curves test. A square pulse of ± 4.5 V amplitude and 200 μs width was used for the endurance test. The PUND was measured using a triangular wave of 4.5 V amplitude at 200 μs pulse width. The threshold voltage was extracted by the linear extrapolation method. The interfacial density (D_{it}) was measured by the conductance method.

B. Direct extraction of trapped charges

The direct measurement of trapped charges has been given in our previous work [19]. The main theory of this measurement method is described as follows. Generally, electrons are trapped into the gate stack after program (PGM) pulse, and here the trapped charge amount is denoted as $Q_{t,PGM}$. Holes are trapped after erase (ERS) pulse, and the trapped charge amount is denoted as $Q_{t,ERS}$. We experimentally measure the difference between the $Q_{t,PGM}$ and $Q_{t,ERS}$, i.e., $\Delta Q_t = Q_{t,PGM} - Q_{t,ERS}$ in this work, which represents the charge trapping behavior.

According to the charge neutrality condition, we can obtain

$$\Delta Q_t = -(\Delta Q_m + \Delta Q_{Si})$$

where the ΔQ_m is the charge change on the metal gate, and ΔQ_{Si} is the charge change on the substrate. For the ΔQ_m , we can obtain it by integrating the external circuit gate current. For the substrate charges ΔQ_t , it is equal to the difference of the C_g-V_g curve integral from 0 to the respective threshold voltage (V_{th}) after positive and negative pulses, that is

$$\begin{aligned} \Delta Q_{Si} &= \int_0^{V_{th,PGM}} C_{g,PGM}(V_g) dV_g - \int_0^{V_{th,ERS}} C_{g,ERS}(V_g) dV_g \\ &= \int_{\Delta V_{th}}^{V_{th,ERS}} C_{g,ERS}(V_g) dV_g - \int_0^{V_{th,ERS}} C_{g,PGM}(V_g) dV_g \\ &= -\int_0^{\Delta V_{th}} C_{g,ERS}(V_g) dV_g \end{aligned}$$

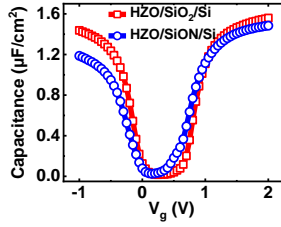


Fig. 4. The C_g - V_g curves of FeFET with SiO_2 and SiON .

Thus, the trapped charges ΔQ_t can be obtained when the ΔQ_m and ΔQ_{Si} are obtained. The details of this method can be found in ref. [19].

III. RESULTS AND DISCUSSION

A. Different interlayers

Fig. 4 shows the C_g - V_g curves of FeFET with SiO_2 and SiON . During measurement, the source, drain, and bulk were connected as a terminal, while the gate was the other terminal. The equivalent oxide thickness (EOT) of SiON and SiO_2 samples are 19.5 Å and 18.2 Å, respectively. Then the dielectric constant of SiON can be obtained as follows [23]

$$\kappa_{\text{SiON}} = \kappa_{\text{SiO}_2} \times \frac{t_{\text{SiON}}}{t_{\text{SiO}_2} - \delta_{\text{EOT}}}$$

where κ_{SiON} and κ_{SiO_2} are the dielectric constants of SiON and SiO_2 , respectively; t_{SiON} and t_{SiO_2} represent the physical thicknesses of SiON and SiO_2 , respectively; δ_{EOT} is the EOT difference between these two interlayers. Finally, the κ_{SiON} is determined to be 4.7. This value is consistent with the reported results [31, 32].

Fig. 5(a) and (b) show the I_d - V_g curves of SiO_2 and SiON samples after wake up, respectively. The memory window (MW) is nearly the same, i.e., 1.54 V and 1.56 V. Figs. 5(c)-(f) show the I_d - V_g curves of SiO_2 and SiON samples during the endurance process. The subthreshold swing (SS) degrades during the endurance fatigue, indicating that the D_{it} is increasing.

The I_d - V_g degradation is different between the SiO_2 and SiON samples. The initial $I_{on}@V_g=V_{th}+1.0$ V of the SiO_2 sample is 3.11 $\mu\text{A}/\mu\text{m}$, and it decreases to 31.3% and 11.7% after the first PGM and ERS operation, respectively. In contrast, the initial $I_{on}@V_g=V_{th}+1.0$ V of the SiON sample is 3.14 $\mu\text{A}/\mu\text{m}$, and it decreases to 96.9% and 43.9% after the first PGM and ERS operation, respectively. Thus, the I_{on} degradation is more severe for the SiO_2 sample. The physical origin of I_{on} degradation after PGM/ERS operation is Coulomb scattering from increased trapped charges at $\text{Hf}_{0.5}\text{Zr}_{0.5}\text{O}_2$ /interlayer interface and interfacial charges at interlayer/Si interface, which will be discussed later.

The V_{th} can be extracted and the endurance characteristics of FeFET with different interlayers are shown in Fig. 6(a). The MW decreases with increasing the PGM/ERS cycle. The endurance of the SiON sample reaches 10^5 cycles, which is 10 times larger than that of the SiO_2 sample. In addition, the initial MW of the SiON sample is 1.56 V. The above result is similar to the reported result [12].

We quantitatively investigate the charge trapping behavior. Fig. 6(b) shows the measured trapped charges into the gate stack as a function of the cycle number. It can be seen that the

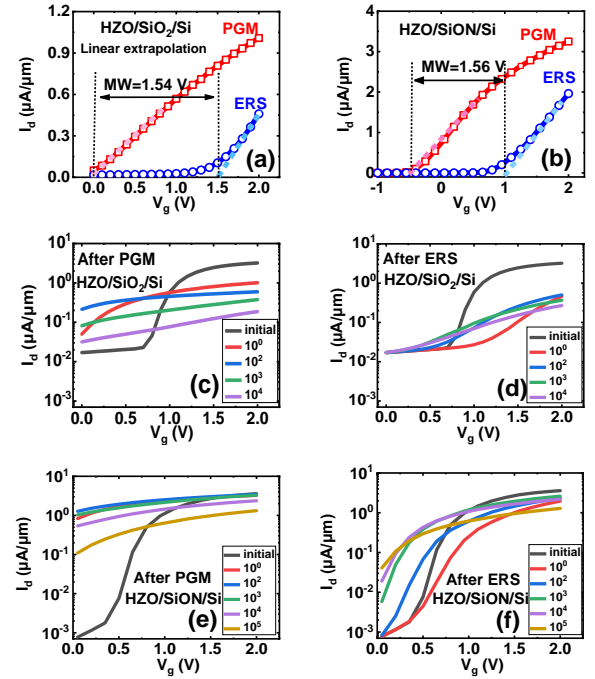


Fig. 5. (a) and (b) show the I_d - V_g curves of SiO_2 and SiON samples after wake up, respectively. The I_d - V_g curves during the endurance fatigue are given in (c) and (d) for the SiO_2 sample, and (e) and (f) for the SiON sample. Gate length/width is 5/150 μm for all the devices, and $V_d=100$ mV for I_d - V_g measurement.

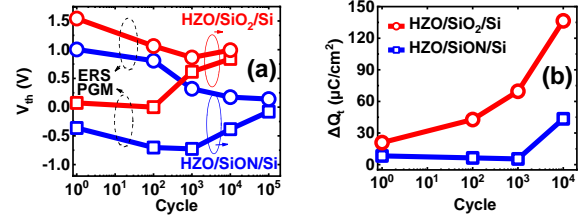


Fig. 6. (a) The endurance characteristics of FeFET with different interlayers and (b) the trapped charges during the cycling.

trapped charges of the SiON sample are always lower than that of the SiO_2 sample. In addition, the trapped charges of the SiON sample increase slower than that of the SiO_2 sample as the PGM/ERS cycle increases. Moreover, when the PGM/ERS cycle increases from 10^0 to 10^4 , the trapped charges of SiON sample increase to 43.5 $\mu\text{C}/\text{cm}^2$, which is smaller than SiO_2 sample (136.5 $\mu\text{C}/\text{cm}^2$). This indicates that more traps have been generated for the SiO_2 sample. Considering that the charge trapping/de-trapping occurs from the Si substrate into $\text{Hf}_x\text{Zr}_{1-x}\text{O}_2$ /interlayer interface, these results indicate that the introduction of N element into the SiO_2 interlayer can effectively suppress charge trapping and trap generation at $\text{Hf}_x\text{Zr}_{1-x}\text{O}_2$ /Si interface. It should be noted that it is the first time that the charge trapping behavior is experimentally extracted for the SiON sample and that the charge trapping behavior is directly verified to be effectively suppressed compared with the SiO_2 sample.

We next investigate the D_{it} . Fig. 7 shows the averaged D_{it} across the bandgap after the erase operation as a function of the cycle number. It can be seen that the D_{it} of the SiO_2 sample increases rapidly, from 10^{13} $\text{eV}^{-1}\cdot\text{cm}^{-2}$ to 10^{14} $\text{eV}^{-1}\cdot\text{cm}^{-2}$ as the PGM/ERS cycle increases from 10^0 to 10^4 . Whereas the D_{it} of

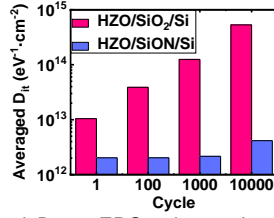


Fig. 7. The averaged D_{it} vs. ERS pulse cycle of FeFET devices with different interlayers.

the SiON sample is much lower, and it is nearly unchanged until the 10^3 cycles. This proves that the introduction of the N element can effectively suppress the D_{it} generation in FeFET. Nitrogen incorporation is well known to strengthen the SiO₂/Si interface by passivating dangling bonds and forming a stronger bond with Si [10]. Therefore, the introduction of the N element can effectively suppress trap generation both at the Hf_xZr_{1-x}O₂/SiO₂ and SiO₂/Si interfaces.

We discuss the energy position of traps at the Hf_{0.5}Zr_{0.5}O₂/SiO₂ interface. The endurance fatigue of SiO₂ and SiON samples is due to the V_{th} increase after PGM and decrease after ERS. Considering that the trapped charges increase during endurance fatigue, we can conclude that the generated traps are localized both near the conduction band and valence band.

B. Hf_xZr_{1-x}O₂ with different Hf:Zr ratios

We investigate the impact of Hf_xZr_{1-x}O₂ with different Hf:Zr ratios on the endurance characteristics. Firstly, we investigate the MFM capacitors. Fig. 8(a) shows initial polarization-voltage (P - V) curves of MFM capacitors. It can be seen that the Hf:Zr ratio effectively tunes the P - V curve. Fig. 8(b) shows endurance characteristics of the MFM capacitors with different Hf:Zr ratios. All the samples reach an endurance of 10^5 ~ 10^7 cycles. The coercive voltage (V_c) and saturated spontaneous polarization (P_s) are summarized as shown in Fig. 8(c) and (d), respectively. It can be seen that for samples Hf_{0.5}Zr_{0.5}O₂, Hf_{0.6}Zr_{0.4}O₂, and Hf_{0.75}Zr_{0.25}O₂, the initial values of $2V_c$ are similar and about 1.5 V, while the $2P_s$ decreases from 51.8 $\mu\text{C}/\text{cm}^2$ to 16.2 $\mu\text{C}/\text{cm}^2$.

Secondly, we investigate the FeFET with different Hf:Zr ratios. Fig. 9 shows the initial I_d - V_g curves, together with those after the 10^0 PGM/ERS cycle. The I_d - V_g degradation is observed. The initial $I_{on}@V_g=V_{th}+1.0$ V for all samples is ~3.0 $\mu\text{A}/\mu\text{m}$. After the first PGM and ERS operation, I_{on} decreases to 31.4% and 14.3% for Hf_{0.5}Zr_{0.5}O₂ sample, 46.3% and 28.8% for Hf_{0.6}Zr_{0.4}O₂ sample, 81.4% and 79.5% for Hf_{0.75}Zr_{0.25}O₂ sample. The physical origin of I_{on} degradation after PGM/ERS operation is Coulomb scattering from increased trapped

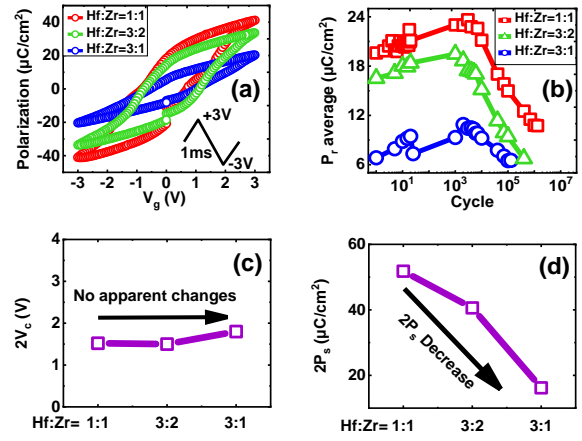


Fig. 8. (a) The initial P - V curves and (b) the fatigue characteristics of MFM capacitors with different Hf:Zr ratios. The P_r means remanent polarization. (c) The initial $2V_c$ and (d) the initial $2P_s$ of MFM capacitors vs. different Hf:Zr ratios.

charges and D_{it} . The subthreshold swing also degrades during the endurance fatigue, indicating that the D_{it} is increasing.

The V_{th} can be extracted and the MW is shown in Fig. 10. The endurance of all samples is ~ 10^4 cycles. After 10^4 cycles, the gate stack breakdown occurs. Therefore, we use the MW degradation percent from 10^0 to 10^3 cycles to compare the endurance characteristics, as shown in Fig. 10(d). As the P_s decrease from 25.9 $\mu\text{C}/\text{cm}^2$ of Hf_{0.5}Zr_{0.5}O₂ to 20.3 $\mu\text{C}/\text{cm}^2$ of Hf_{0.6}Zr_{0.4}O₂, the endurance characteristics improve. In contrast, when the P_s further decreases from 20.3 $\mu\text{C}/\text{cm}^2$ of Hf_{0.6}Zr_{0.4}O₂ to 8.1 $\mu\text{C}/\text{cm}^2$ of Hf_{0.75}Zr_{0.25}O₂, the endurance characteristics degrade.

Then we quantitatively investigate the charge trapping behavior. Fig. 11(a) shows the measured trapped charges into the gate stack as a function of the cycle number. It can be seen that the trapped charges decrease in the sequence of Hf_{0.5}Zr_{0.5}O₂, Hf_{0.6}Zr_{0.4}O₂, and Hf_{0.75}Zr_{0.25}O₂, which is the same as the changing trend of P_s . Especially the charge trapping behavior nearly disappears for the Hf_{0.75}Zr_{0.25}O₂ sample. Therefore, decreasing the ferroelectric P_s can effectively suppress the charge trapping.

However, as shown in Fig. 11(b), as the charge trapping effect becomes weakened, the endurance characteristics initially improve and then degrade. Moreover, it is worthy to note that the initial MW of the Hf_{0.75}Zr_{0.25}O₂ sample is nearly zero, and MW is all negative after 10^0 PGM/ERS cycle, even though the $2E_c$ of Hf_{0.75}Zr_{0.25}O₂ sample is similar to others. We discuss the physical origin by analyzing the relationship among the

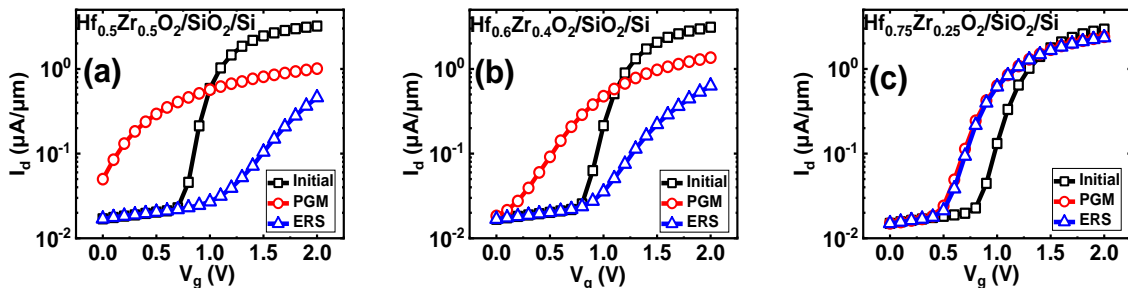


Fig. 9. The initial I_d - V_g curves and the I_d - V_g curves after the 1 cycle of PGM/ERS operation for FeFET with different Hf:Zr. Gate length/width is 5/150 μm for all the devices, and $V_r=100$ mV for I_d - V_g measurement.

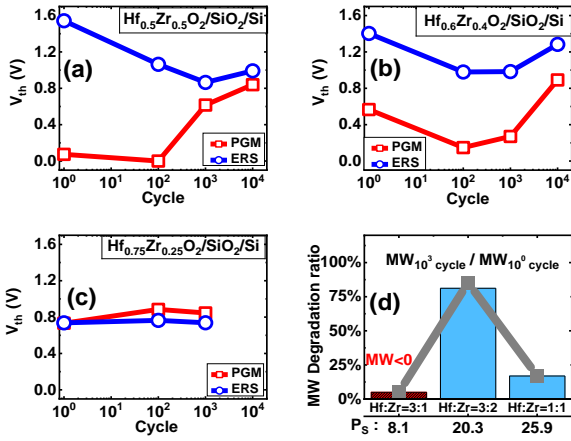


Fig. 10. (a)-(c) The endurance characteristics of FeFET with different Hf:Zr ratios. (d) MW degradation ratio (10³ cycles to 10⁴ cycles) vs. Hf:Zr ratio.

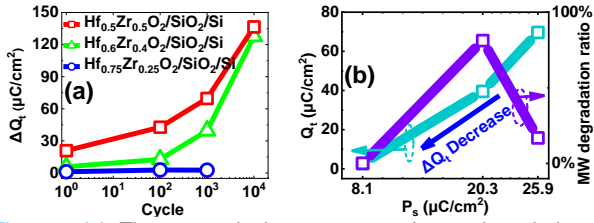


Fig. 11. (a) The trapped charges vs. cycle number during the endurance process for FeFET with different Hf:Zr ratios. (b) The ΔQ_t and endurance characteristics in 10³ cycles vs. the P_s .

polarization, charge trapping, and the MW as follows.

Firstly, we discuss the endurance improvement from $\text{Hf}_{0.5}\text{Zr}_{0.5}\text{O}_2$ to $\text{Hf}_{0.6}\text{Zr}_{0.4}\text{O}_2$ samples. Fig. 12 shows the ferroelectric hysteresis loop and loadline of the MFIS gate stack for the three samples. All the curve numbers are labeled as 1, 2, and 3 for the $\text{Hf}_{0.5}\text{Zr}_{0.5}\text{O}_2$ sample ($P_s=25.9 \mu\text{C}/\text{cm}^2$), the $\text{Hf}_{0.6}\text{Zr}_{0.4}\text{O}_2$ sample ($P_s=20.3 \mu\text{C}/\text{cm}^2$), and the $\text{Hf}_{0.75}\text{Zr}_{0.25}\text{O}_2$ sample ($P_s=8.1 \mu\text{C}/\text{cm}^2$), respectively. By reducing the P_s , the V_{IL} and consequent E_{IL} decrease at the same applied gate voltage (from $V_{IL,1}$ to $V_{IL,2}$). Thus, the endurance improves. In addition, the MW decreases from $\text{Hf}_{0.5}\text{Zr}_{0.5}\text{O}_2$ to $\text{Hf}_{0.6}\text{Zr}_{0.4}\text{O}_2$ sample as shown in Fig. 10. This is explained as follows. At $V_g=V_{th}$, the substrate charge is defined as $Q_{Si,th}$. For the case without charge trapping, the charges in the metal gate corresponding to V_{th} are equal to $Q_{Si,th}$, which is shown as the dash lined ‘TH0’ in Fig. 12(a). When charge trapping appears, at $V_g=V_{th}$, the charges in the metal gate corresponding to V_{th} are equal to $Q_{Si,th}+Q_t$, which is shown as the dashed line ‘TH1’.

Then the MW can be determined to be the distance between the intersections of the hysteresis loop and the line ‘TH1’. When ferroelectric material changes from $\text{Hf}_{0.5}\text{Zr}_{0.5}\text{O}_2$ to $\text{Hf}_{0.6}\text{Zr}_{0.4}\text{O}_2$, the P_s reduces and the hysteresis loop changes from the line ‘HL1’ to the line ‘HL2’. The trapped charges slightly reduce and the line representing V_{th} changes from the line ‘TH1’ to the line ‘TH2’. Because the P_s reduction is larger than the trapped charge reduction, the line ‘HL2’ drops more than the line ‘TH2’ as shown in Fig. 12(b). Therefore, the MW decreases.

Secondly, we discuss the MW of $\sim 0.02 \text{ V}$ for $\text{Hf}_{0.75}\text{Zr}_{0.25}\text{O}_2$ sample ($P_s=8.1 \mu\text{C}/\text{cm}^2$). Due to the small P_s , the intersections between the hysteresis loop line ‘HL3’ and line ‘TH3’ can be localized in the upper right section as shown in Fig. 12(c). Thus, the MW can be significantly reduced.

From the above discussion, it can be concluded that the reduction of P_s could improve endurance characteristics. On the contract, it can also reduce the MW. The above two points are determined by the competition between P_s reduction and charge trapping induced by it. Therefore, the impact of P_s reduction on endurance fatigue needs careful consideration.

IV. CONCLUSION

We study the impact of different interlayers and ferroelectric materials on charge trapping during the endurance fatigue of Si FeFET with $\text{Hf}_x\text{Zr}_{1-x}\text{O}_2$ /interlayer gate stack and analyze the endurance degradation mechanism caused by the charge trapping. We directly extract the charge trapping behavior for SiO_2 and SiON interlayer for the first time. The introduction of the N element in the SiO_2 interlayer effectively suppresses the charge trapping and defect generation and improves the endurance characteristics. By reducing the saturated spontaneous polarization of ferroelectric, the charge trapping can be effectively suppressed, and the endurance characteristics can also be improved. However, it can also cause MW degradation. Our work helps design the MFIS gate stack.

REFERENCES

- [1] T. S. Böske *et al.*, "Ferroelectricity in hafnium oxide: CMOS compatible ferroelectric field effect transistors," in *2011 International Electron Devices Meeting*, 2011, pp. 24.5.1-24.5.4. doi:10.1109/IEDM.2011.6131606.
- [2] J. Müller *et al.*, "Ferroelectric hafnium oxide: A CMOS-compatible and highly scalable approach to future ferroelectric memories," in *2013 IEEE International Electron Devices Meeting*, 2013, pp. 10.8.1-10.8.4. doi:10.1109/IEDM.2013.6724605.
- [3] M. Trentzsch *et al.*, "A 28nm HKMG super low power embedded NVM technology based on ferroelectric FETs," in *2016 IEEE International Electron Devices Meeting (IEDM)*, 2016, pp. 11.5.1-11.5.4.

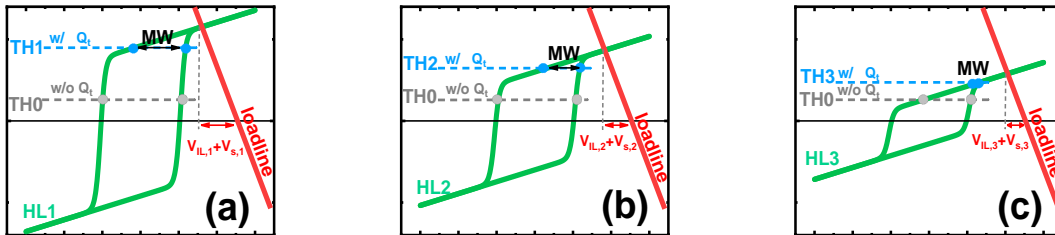


Fig.12. Ferroelectric hysteresis loop and Loadline simulation model of memory window and endurance characteristics changing with the ferroelectric reduction.

- doi:10.1109/IEDM.2016.7838397.
- [4] K. T. Chen *et al.*, "Non-Volatile Ferroelectric FETs Using 5-nm $\text{Hf}_{0.5}\text{Zr}_{0.5}\text{O}_2$ With High Data Retention and Read Endurance for 1T Memory Applications," *IEEE Electron Device Letters*, vol. 40, no. 3, pp. 399-402, 2019. doi:10.1109/led.2019.2896231.
- [5] A. A. Sharma *et al.*, "High Speed Memory Operation in Channel-Last, Back-gated Ferroelectric Transistors," in *2020 IEEE International Electron Devices Meeting (IEDM)*, 2020, pp. 18.5.1-18.5.4. doi:10.1109/IEDM13553.2020.9371940.
- [6] Y.-H. Chen *et al.*, "Improved TDDB Reliability and Interface States in 5-nm $\text{Hf}_{0.5}\text{Zr}_{0.5}\text{O}_2$ Ferroelectric Technologies Using NH_3 Plasma and Microwave Annealing," *IEEE Transactions on Electron Devices*, vol. 67, no. 4, pp. 1581-1585, 2020. doi:10.1109/ted.2020.2973652.
- [7] H. Mulaosmanovic *et al.*, "Recovery of Cycling Endurance Failure in Ferroelectric FETs by Self-Heating," *IEEE Electron Device Letters*, vol. 40, no. 2, pp. 216-219, 2019. doi:10.1109/led.2018.2889412.
- [8] S. Oh *et al.*, "Improved Endurance of HfO_2 -Based Metal-Ferroelectric-Insulator-Silicon Structure by High-Pressure Hydrogen Annealing," *IEEE Electron Device Letters*, vol. 40, no. 7, pp. 1092-1095, 2019. doi:10.1109/led.2019.2914700.
- [9] H.-K. Peng *et al.*, "Enabling large memory window and high reliability for FeFET memory by integrating AION interfacial layer," *Applied Physics Letters*, vol. 118, no. 10, 2021. doi:10.1063/5.0036824.
- [10] T. Ali *et al.*, "High Endurance Ferroelectric Hafnium Oxide-Based FeFET Memory Without Retention Penalty," *IEEE Transactions on Electron Devices*, vol. 65, no. 9, pp. 3769-3774, 2018. doi:10.1109/ted.2018.2856818.
- [11] T. Ali *et al.*, "A Multilevel FeFET Memory Device based on Laminated HSO and HZO Ferroelectric Layers for High-Density Storage," in *2019 IEEE International Electron Devices Meeting (IEDM)*, 2019, pp. 28.7.1-28.7.4. doi:10.1109/IEDM19573.2019.8993642.
- [12] H. Bae *et al.*, "Sub-ns Polarization Switching in 25nm FE FinFET toward Post CPU and Spatial-Energetic Mapping of Traps for Enhanced Endurance," in *2020 IEEE International Electron Devices Meeting (IEDM)*, 2020, pp. 31.3.1-31.3.4. doi:10.1109/IEDM13553.2020.9372076.
- [13] A. J. Tan *et al.*, "Hot Electrons as the Dominant Source of Degradation for Sub-5nm HZO FeFETs," in *2020 IEEE Symposium on VLSI Technology*, 2020, pp. 1-2. doi:10.1109/VLSITechnology18217.2020.9265067.
- [14] S. Agarwal *et al.*, "International Roadmap of Devices and Systems 2020 Edition: Beyond CMOS chapter". <https://irds.ieee/>
- [15] X. F. Zheng *et al.*, "Electron Trapping in HfAlO High- κ Stack for Flash Memory Applications: An Origin of V_{th} Window Closure During Cycling Operations," *IEEE Transactions on Electron Devices*, vol. 58, no. 5, pp. 1344-1351, 2011. doi:10.1109/ted.2011.2115244.
- [16] E. Yurchuk *et al.*, "Charge-Trapping Phenomena in HfO_2 -Based FeFET-Type Nonvolatile Memories," *IEEE Transactions on Electron Devices*, vol. 63, no. 9, pp. 3501-3507, 2016. doi:10.1109/ted.2016.2588439.
- [17] B. Zeng *et al.*, "Program/Erase Cycling Degradation Mechanism of HfO_2 -Based FeFET Memory Devices," *IEEE Electron Device Letters*, vol. 40, no. 5, pp. 710-713, 2019. doi:10.1109/led.2019.2908084.
- [18] N. Gong and T.-P. Ma, "A Study of Endurance Issues in HfO_2 -Based Ferroelectric Field Effect Transistors: Charge Trapping and Trap Generation," *IEEE Electron Device Letters*, vol. 39, no. 1, pp. 15-18, 2018. doi:10.1109/led.2017.2776263.
- [19] S. Zhao *et al.*, "Experimental Extraction and Simulation of Charge Trapping during Endurance of FeFET with TiN/HfZrO/SiO₂/Si (MFIS) Gate Structure," *arXiv e-prints*, p. arXiv:2106.15939, 2021.
- [20] A. J. Tan *et al.*, "A Nitrided Interfacial Oxide for Interface State Improvement in Hafnium Zirconium Oxide-Based Ferroelectric Transistor Technology," *IEEE Electron Device Letters*, vol. 39, no. 1, pp. 95-98, 2018. doi:10.1109/LED.2017.2772791.
- [21] T. Jung *et al.*, "Impact of interface layer on charge trapping in Si:HfO₂ based FeFET," in *2020 IEEE International Integrated Reliability Workshop (IIRW)*, 2020, pp. 1-6. doi:10.1109/IIRW49815.2020.9312866.
- [22] C. Y. Chan *et al.*, "FeFET Memory Featuring Large Memory Window and Robust Endurance of Long-Pulse Cycling by Interface Engineering using High- κ AION," in *2020 IEEE Symposium on VLSI Technology*, 2020, pp. 1-2. doi:10.1109/VLSITechnology18217.2020.9265103.
- [23] A. J. Tan *et al.*, "Ferroelectric HfO_2 Memory Transistors with High- κ Interfacial Layer and Write Endurance Exceeding 10^{10} Cycles," *IEEE Electron Device Letters*, pp. 1-1, 2021. doi:10.1109/LED.2021.3083219.
- [24] K. Ni *et al.*, "SoC Logic Compatible Multi-Bit FeMFET Weight Cell for Neuromorphic Applications," in *2018 IEEE International Electron Devices Meeting (IEDM)*, 2018, pp. 13.2.1-13.2.4. doi:10.1109/IEDM.2018.8614496.
- [25] P. D. Lomenzo *et al.*, "Ferroelectric Si-Doped HfO_2 Device Properties on Highly Doped Germanium," *IEEE Electron Device Letters*, vol. 36, no. 8, pp. 766-768, 2015. doi:10.1109/LED.2015.2445352.
- [26] J. H. Bae *et al.*, "Highly Scaled, High Endurance, Ω -Gate, Nanowire Ferroelectric FET Memory Transistors," *IEEE Electron Device Letters*, vol. 41, no. 11, pp. 1637-1640, 2020. doi:10.1109/LED.2020.3028339.
- [27] K. Lee *et al.*, "Ferroelectric-Gate Field-Effect Transistor Memory With Recessed Channel," *IEEE Electron Device Letters*, vol. 41, no. 8, pp. 1201-1204, 2020. doi:10.1109/LED.2020.3001129.
- [28] T. Kim *et al.*, "High-Performance and High-Endurance HfO_2 -Based Ferroelectric Field-Effect Transistor Memory with a Spherical Recess Channel," (in English), *Physica Status Solidi-Rapid Research Letters*, vol. 15, no. 5, p. 2100018, May 2021. doi:10.1002/pssr.202100018.
- [29] S. Deng *et al.*, "Guidelines for Ferroelectric FET Reliability Optimization: Charge Matching," *IEEE Electron Device Letters*, vol. 41, no. 9, pp. 1348-1351, 2020. doi:10.1109/LED.2020.3011037.
- [30] J. Muller *et al.*, "High endurance strategies for hafnium oxide based ferroelectric field effect transistor," in *2016 16th Non-Volatile Memory Technology Symposium (NVMTS)*, 2016, pp. 1-7. doi:10.1109/NVMTS.2016.7781517.
- [31] J. Robertson, "High dielectric constant oxides," *The European Physical Journal Applied Physics*, vol. 28, no. 3, pp. 265-291, 2004. doi:10.1051/epjap:2004206.
- [32] N. Konofaos, "Electrical characterisation of SiON/n-Si structures for MOS VLSI electronics," *Microelectronics Journal*, vol. 35, no. 5, pp. 421-425, 2004. doi:10.1016/j.mejo.2004.01.001.